

The Excess Far-Infrared Emission of AGN in the Local Universe

A. Pasquali,^{1*} G. Kauffmann,² T.M. Heckman,³

¹*Institute of Astronomy, ETH Hoenggerberg, HPF, 8093 Zurich, Switzerland*

²*Max-Planck-Institut für Astrophysik, Karl Schwarzschild Str. 1, 85748 Garching, Germany*

³*Center for Astrophysical Sciences, Department of Physics and Astronomy, Johns Hopkins University, Baltimore, MD, 21218 USA*

ABSTRACT

We have cross-correlated the Sloan Digital Sky Survey (SDSS) second data release spectroscopic galaxy sample with the IRAS faint-source catalogue (FSC). Optical emission line ratios are used to classify the galaxies with reliable IRAS 60 and 100 μm detections into AGN and normal star-forming galaxies. We then create subsamples of normal galaxies and AGN that are very closely matched in terms of key physical properties such as stellar mass, redshift, size, concentration and mean stellar age (as measured by absorption line indicators in the SDSS spectra). We then quantify whether there are systematic differences between the IR luminosities of the galaxies and the AGN in the matched subsamples. We find that the AGN exhibit a significant excess in far-IR emission relative to the star-forming galaxies in our sample. The excesses at 60 μm and 100 μm are 0.21 ± 0.03 dex and 0.12 ± 0.035 dex in $\log L_{60}/M_*$ and $\log L_{100}/M_*$, respectively. We then discuss whether the far-IR excess is produced by radiation from the active nucleus that is absorbed by dust or alternatively, by an extra population of young stars that is not detectable at optical wavelengths.

Key words: galaxies:active; galaxies:Seyfert; galaxies:starburst; galaxies:stellar contentx

1 INTRODUCTION

In the mid 1980’s, spectroscopic follow up of galaxies observed by the IRAS satellite revealed that infrared-luminous galaxies consist of a mixture of star-forming galaxies and galaxies with an active nucleus (AGN). De Grijp et al. (1985) found that fraction of AGN could be maximized by selecting IRAS sources with relatively warm 25 to 60 micron colours and they then used this criterion to construct a catalog of 80 Seyfert 1 and 141 Seyfert 2 galaxies (De Grijp et al. 1992).

A considerable amount of effort has been devoted to understanding the physical mechanisms responsible for the infrared emission in AGN. The current paradigm asserts that type 1 and type 2 Seyfert galaxies are drawn from the same parent population. In type 1 Seyfert galaxies the subparsec-scale continuum source is viewed directly, but in type 2 Seyferts this source is blocked from view by a structure (commonly referred to as the “torus”) with a size of between 1 and 10 parsec, which is optically thick to radiation from X-ray to near-IR wavelengths. The size of the obscuring region, together with energy conservation arguments, then imply that most of the radiation absorbed by

this structure will be re-radiated in the mid-IR as thermal emission from dust (Pier & Krolik 1992; Granato & Danese 1994).

In recent years it has become clear that star formation and AGN activity frequently occur together in galaxies (e.g. Cid Fernandes et al. 2001; Kauffmann et al. 2003c; Heckman et al. 2004). As a result, it is natural to suppose that a substantial fraction of IR emission from AGN may be produced by star formation. It is commonly believed that star formation is likely to dominate the emission at long wavelengths ($> 60\mu\text{m}$) and that emission from the torus prevails in the mid-IR. Rowan-Robinson & Crawford (1989) modelled the far-IR spectra of IRAS galaxies using three components: a “disc component” due to the interstellar dust illuminated by the galaxy’s starlight; a “starburst component” arising from hot stars in optically thick dust clouds, and a “Seyfert component” due to a power-law continuum source within the torus. In most cases ($\sim 61\%$), the IRAS spectra are well fitted by a combination of disc and starburst components. Only $\sim 24\%$ of the galaxies in the samples required the Seyfert component. Nevertheless, as discussed by Silva, Granato & Maiolino (2004), the intrinsic far-IR properties of AGN remain subject to strong uncertainties (only large-aperture data from ISO or IRAS are available at $\lambda > 20\mu\text{m}$)

* Email: pasquali@phys.ethz.ch

and there is also substantial freedom in the dusty torus models at these wavelengths.

The relative importance of dust heating by star formation and by AGN has also been a topic of considerable controversy in the study of ultraluminous IRAS galaxies (ULIRGs), which are the most powerful galaxies detected by IRAS with IR luminosities in excess of $10^{12}L_{\odot}$. A significant fraction of ULIRGs exhibit nuclear optical emission line spectra characteristic of Seyfert galaxies (Sanders et al. 1988; Armus et al. 1990), but the infrared, millimeter and radio characteristics of these systems are very similar to those of ordinary starbursts (Rieke et al. 1985; Rowan-Robinson & Crawford 1989; Condon et al. 1991). Genzel et al. (1998) used mid-infrared spectra from the ISO satellite to demonstrate that 70-80% of the ULIRGs in their sample were predominantly powered by star formation and 20-30% by a central AGN. These conclusions were based on an analysis of the ratio of high- to low-excitation mid-IR emission lines as well as the strength of the $7.7 \mu\text{m}$ PAH feature in these systems.

The same question is relevant when attempting to convert from the luminosity function of sub-millimeter sources observed at high redshifts to estimates of the total star formation rate density (e.g. Blain et al. 1999; Rowan-Robinson 2001). The contribution from AGN has been investigated by looking for overlap between sub-mm galaxies detected by SCUBA and hard X-ray sources found by Chandra. Only around 10% of the sub-mm sources are found to have an X-ray counterpart (Severgnini et al. 2000; Barger et al. 2001). More recently Silva et al. (2004) have used a combination of X-ray data on the evolution of the AGN luminosity function and spectral energy distributions drawn from their models to show that around 95% of the total IR background is likely produced by star formation.

In this paper, we study the far-infrared properties of AGN in the local Universe. As a result of recent large redshift surveys such as the Sloan Digital Sky Survey (SDSS), it is possible to compile unprecedentedly large samples of galaxies with both high quality optical spectra and IRAS fluxes. It then becomes possible to adopt a purely statistical approach to understanding the origin of the IR emission in AGN. In this paper, we analyze a sample of over a thousand galaxies drawn from the SDSS Data Release 2 (DR2) with IRAS detections. Optical emission line ratios are used to classify the galaxies into AGN and “normal” galaxies. We then create subsamples of normal galaxies and AGN that have been carefully matched in terms of key physical properties such as stellar mass, redshift, galaxy structural parameters and mean stellar age, and we quantify whether there are systematic differences between the mean IR luminosities of the galaxies in the matched subsamples.

2 THE GALAXY SAMPLES

2.1 The SDSS Spectroscopic Sample

The Sloan Digital Sky Survey (York et al. 2000; Stoughton et al. 2002, and references therein) is an optical imaging (u,g,r,i,z bands) and spectroscopic survey of about a quarter of the extragalactic sky, being carried out at the Apache Point Observatory. The spectroscopic sample considered in

this paper is a sample of about 212,000 objects with magnitudes $14.5 < r < 17.77$, spectroscopically confirmed to be galaxies. This sample of galaxies is described by Brinchmann et al. (2004). The galaxies have a median redshift of $z \sim 0.1$.

The SDSS spectra cover an observed wavelength range of 3800 to 9200Å, at an instrumental velocity resolution of about 65km s^{-1} . The spectra are obtained through fibres of about 3-arcsecond diameter, which corresponds to 5.7 kpc at a redshift of 0.1; at this redshift the spectra therefore represent a large proportion (up to 50%) of the total galaxy light, whilst for the very lowest redshift objects they are more dominated by the nuclear emission.

As described by Brinchmann et al. (2004), many properties of these galaxies have been parameterised, with the derived catalogues of parameters being publically available on the web. Derived parameters include: fundamental galaxy parameters such as total stellar masses, sizes, surface mass densities, concentration indices, mass-to-light ratios, 4000Å break strengths, dust attenuation measurements, and H δ absorption measurements (Kauffmann et al. 2003a); accurate emission line fluxes, after subtraction of the modelled stellar continuum to account for underlying stellar absorption features (Kauffmann et al. 2003a; Tremonti et al. 2004); galaxy metallicities (Tremonti et al. 2004); star formation rates (Brinchmann et al. 2004); parameters measuring optical AGN activity, such as emission line ratios, and galaxy velocity dispersions (hence black hole mass estimates; Kauffmann et al. 2003c, Heckman et al. 2004). The sample analysed in this paper includes star-forming galaxies and those AGN in which non-stellar continuum light from the nucleus has a negligible effect on the physical parameters derived for the host galaxy (see Kauffmann et al. 2003c for more detailed discussion). In the rest of the paper we use the term “AGN” to refer to these objects.¹

2.2 Cross-identification with the IRAS catalogues

We cross-identified the SDSS galaxies with the IRAS Faint-Sources Catalogue (FSC) using the web search engine GATOR (available at <http://irsa.ipac.caltech.edu/applications/Gator>). We initially assumed a search radius of 1 arcmin in order to account for the IRAS positional uncertainties. Initially, no constraint on the IRAS flux density or the quality of the IRAS flux detections was applied and the query returned a total of 5765 matches. Because of the large search radius, a substantial number of IRAS sources (1205 or 21%) were matched to more than one SDSS galaxy. These sources were eliminated from our catalogue in order to maximize the reliability of our sample. Our catalogue is thus incomplete and somewhat biased against galaxies in high density regions, but this is not particularly important for the applications discussed in this paper.

We restricted our analysis to IRAS sources with reliable flux densities [with flux quality from moderate (2) to good (3), which means that they have been detected more than

¹ Note that this sample explicitly excludes those objects classified by the SDSS spectroscopic pipeline as QSOs. In such cases the SDSS spectrum is dominated by light from the AGN.

once in the repeat scans]. As discussed in detail in Kauffmann et al. (2003c), we use the [NII]/H α versus [OIII]/H β emission line ratio diagnostic diagram (Baldwin, Phillips & Terlevich 1981) to classify our galaxies into AGN and normal galaxies. In order for a galaxy to be placed on the BPT diagram, the four emission lines [NII],[OIII],H α and H β must be detected with S/N > 3. Galaxies in which these four lines are not detected with sufficient signal-to-noise are classified as “normal”. The normal galaxy sample may thus contain some AGN with emission lines that are too weak to classify. We are not concerned with this here, because the aim of this paper is to characterize the infrared emission from more powerful Seyfert galaxies. Figure 1 shows the distribution in the BPT diagram of the emission-line galaxies in our sample with 60 and 100 μ m IRAS detections. Red crosses indicate galaxies that are classified as AGN. As can be seen, most of the AGN in our sample lie in the region of the diagram occupied by Seyfert galaxies or by “composite” systems in which there is both an active nucleus and ongoing star formation (see Kauffmann et al. 2003c for a more detailed discussion of how the general population of AGN in the SDSS populate the BPT diagram). There are almost no IRAS-selected AGN in the region of the diagram occupied by LINERs.

The infrared luminosities of the galaxies in our sample were computed using the formulae given in Helou et al. (1988) and Sanders & Mirabel (1996):

$$FIR = 1.26 \times [F(60\mu m) + F(100\mu m)] W m^{-2}$$

$$F(60\mu m) = 2.58 \times 10^{-14} f_{\nu}(60\mu m) W m^{-2}$$

$$F(100\mu m) = 1.00 \times 10^{-14} f_{\nu}(100\mu m) W m^{-2}$$

$$L_{FIR} = 4\pi D_L^2 FIR$$

$$L_{100} = 4\pi D_L^2 F(100\mu m)$$

$$L_{60} = 4\pi D_L^2 F(60\mu m)$$

where $f_{\nu}(60\mu m)$ and $f_{\nu}(100\mu m)$ are the IRAS flux densities and we have adopted a cosmology with $H_0 = 70$ km s $^{-1}$ Mpc $^{-1}$, $\Omega = 0.3$ and $\Lambda = 0.7$

The left panel of Figure 2 shows the FIR luminosities (in solar units) plotted as a function of redshift for all the galaxies with reliable flux measurements at both 60 and 100 μ m. The IRAS flux limit means that the IR luminosities of the objects in our sample increase from $L_{FIR} \simeq 10^{10} L_{\odot}$ at $z = 0.05$ to $\sim 10^{11} L_{\odot}$ at $z = 0.1 - 0.2$. This is true for both normal galaxies and for AGN. In the right panel of Fig. 2, we plot the derived FIR luminosity as a function of the distance in arcseconds between the position of the IRAS source and the position of the matching SDSS galaxy.

2.2.1 Further checks on the reliability of the sample

In our sample, the signal-to-noise of the detected sources ranges from 3.5 up to 50. Follow-up of IRAS FSC sources have shown that at $S/N < 8$, a significant fraction (more than 20%) of the sources turn out to be false detections. Because of the large matching radius that is employed, one might worry that some of these false sources may contaminate our sample. Another source of potential contamination is cirrus emission from interstellar dust in our own Galaxy. In the IRAS catalogue, this is parametrized by the “cirrus flag”, which indicates the number of 100 μ m sources detected within a 30 arcmin radius of the FSC source.

Figure 3 shows the distribution of positional offsets (in arcseconds) between the IRAS FSC source and the matched SDSS galaxy for different cuts in S/N and in cirrus flag. As the S/N of the sources increases there is a slight shift towards smaller offsets, indicating that some false identifications have been eliminated. The shifts are quite small, however, indicating that the majority of low S/N objects are in fact real. Different cuts in the cirrus flag have no effect on the distribution of offsets.

We have generated catalogues of randomly distributed sources in the area of sky covered by DR2 and we use these to evaluate the likelihood that a false detection will be matched with an SDSS galaxy from the main spectroscopic sample. Results are shown in Figure 4 as a function of the matching radius. Since, within the footprint covered by DR2, the FSC contains 4560 sources associated with galaxies, Figure 4 indicates that about 288 false matches occur for a matching radius of 60 arcseconds. At a 30 arcsecond matching radius, the number of randomly matched galaxies drops to about 46, clearly a more acceptable level of contamination. From Figure 3 we see that a cut at a positional offset of 30 arcseconds eliminates only around a quarter of the galaxies in our sample. We conclude that a cut in positional offset is a more efficient way to eliminate contaminating sources than a cut in signal-to-noise.

Another way to evaluate the reliability of the sample is to study the scatter in the relations between properties of galaxies derived from the SDSS spectra and those derived from the IRAS fluxes. In Figure 5 we study the effect of different cuts in positional offset and in redshift on the relation between the 4000 \AA break strength $D_n(4000)$ and the “normalized” FIR luminosity L_{FIR}/M_* . Both quantities are a measure of the age of the stellar population in the galaxy and will be used extensively in the analysis that follows.

In the top panels of Fig. 5, we hold the positional offset cut constant at $R < 30$ arcseconds and we show what happens if different cuts in redshift are imposed on the sample. At high redshifts, the sample contains only extremely IR-luminous objects. Fig. 1 shows there are a handful of galaxies with IR luminosities in excess of $10^{12} L_{\odot}$ at $z > 0.15$. These are the ULIRGs, which have been traditionally considered as a separate class of galaxy in their own right. Since there are very few of these objects in our sample, we exclude them by imposing a cut at $z = 0.15$.

At low redshifts the SDSS spectra, which are obtained using 3 arcsecond diameter fibres, sample only the inner regions of the galaxies and aperture effects may influence our analysis. Kewley, Jansen & Geller (2005) have recently carried out a detailed study of aperture effects on the spectra of galaxies using a sample of 101 nearby galaxies with both global and nuclear spectra. They conclude that so long as the fibre captures more than $\sim 20\%$ of the total light, the differences between physical parameters derived using nuclear spectra and those derived using global spectra are modest. For SDSS, Kewley et al. recommend that redshift cut $z > 0.04$ be imposed. We choose a somewhat more conservative cut ($z > 0.06$). The top panels in Fig. 5 show that this cut eliminates a population of “normal” galaxies with high values of L_{FIR}/M_* . These are primarily low mass galaxies ($< 10^{10} M_{\odot}$) that are currently experiencing a strong burst of star formation. There are very few AGN that have stellar masses lower than $10^{10} M_{\odot}$ (Kauffmann et al. 2003c), so

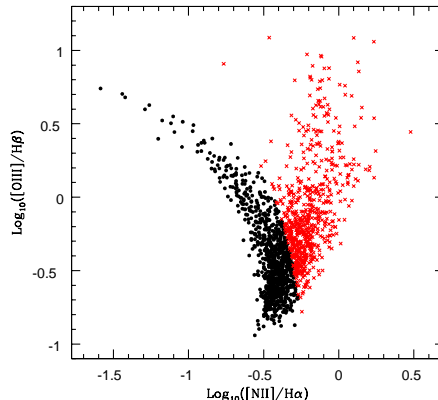


Figure 1. The distribution of IRAS-selected emission-line galaxies in the $[NII]/H\alpha$ versus $[OIII]/H\beta$ BPT diagram. Red crosses indicate objects that are classified as AGN of Type 2.

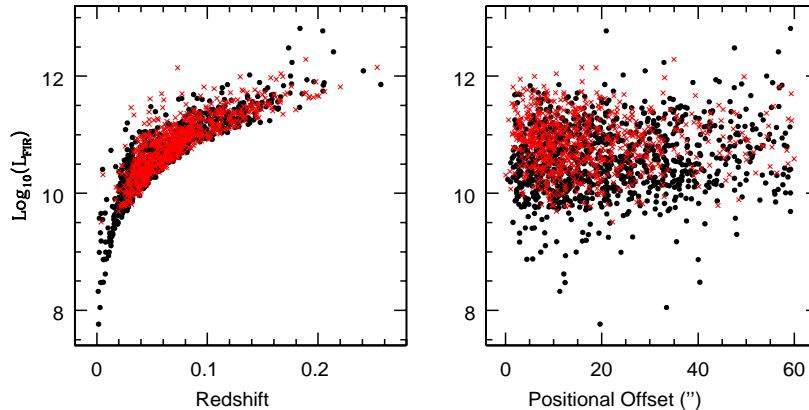


Figure 2. Left: $\text{Log}(L_{FIR})$ is plotted as a function of redshift for AGN of Type 2 (red crosses) and normal star-forming galaxies (black points). Right: $\text{Log}(L_{FIR})$ is plotted as a function of the separation (in arcseconds) between the IRAS source and the matching SDSS galaxy. L_{FIR} is in solar luminosity units.

eliminating these objects from our sample will not affect the analysis presented in this paper.

In the bottom panels, we fix the redshift interval at $0.06 < z < 0.15$ and we investigate what happens if the cut in positional offset is allowed to vary. As can be seen, if matches with positional offsets as large as 60 arcseconds are accepted, there is a “tail” of outlying galaxies with large 4000 \AA break strengths (indicative of an old stellar population), but with high normalized FIR luminosity. These outliers largely disappear when the offset is restricted to be less than 30 arcseconds.

To summarize, the final cuts we impose on our sample are the following:

- (i) Only IRAS sources with flux quality flag ≥ 2 are retained.
- (ii) The positional offset between the IRAS source and the SDSS galaxy must be less than $30''$.
- (iii) All sources that have more than one SDSS match within a matching radius of $30''$ are eliminated.
- (iv) All galaxies with $z < 0.06$ and $z > 0.15$ are also excluded.

We created two catalogues: one with flux measurements at $60 \mu\text{m}$ only (1090 galaxies of which 553 are AGN) and a

second with flux measurements at both 60 and $100 \mu\text{m}$ (526 objects of which 284 are AGN). All sources in the $60 \mu\text{m}$ catalogue have an IRAS flux quality of 3, while all galaxies in the $100 \mu\text{m}$ are characterised by a quality of 2.

3 PROPERTIES OF THE IRAS-SELECTED AGN

In Figure 6 we show the distributions of some of the basic properties of the AGN and the normal star-forming galaxies in our sample, such as their redshifts, IR luminosities, stellar masses, concentrations, stellar surface densities and 4000 \AA break strengths. Unless specified otherwise, we show results for the catalogue with reliable flux measurements at both 60 and $100 \mu\text{m}$. The histograms representing the normal galaxies and the AGN have been shaded in black and in red, respectively.

The main result seen in Figure 6 is that the IRAS-selected AGN have larger stellar masses than the “normal” galaxies in the sample. As discussed by Kauffmann et al. (2003c), the AGN fraction among normal galaxies falls off very steeply at stellar masses less than a few $\times 10^{10} M_{\odot}$ and this is apparent in the third panel of Figure 6. As discussed

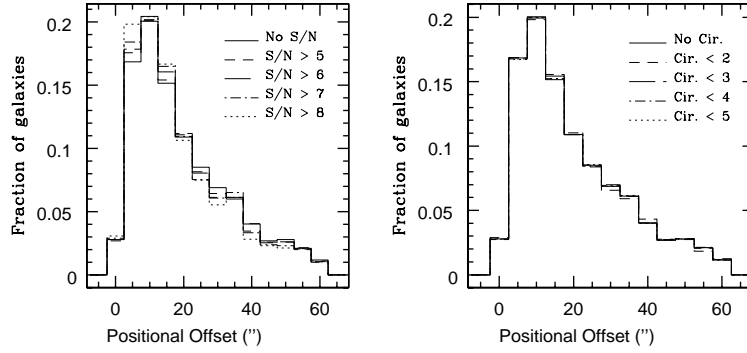


Figure 3. The distribution of positional offset between the FSC source and the matched SDSS galaxy for different cuts in S/N (left) and cirrus flag (right).

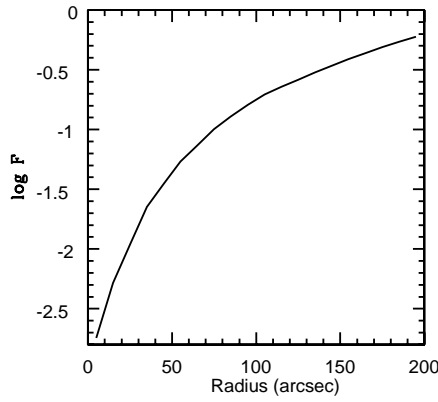


Figure 4. The logarithm of the fraction of randomly placed sources that are matched to an SDSS galaxy as a function of the matching radius.

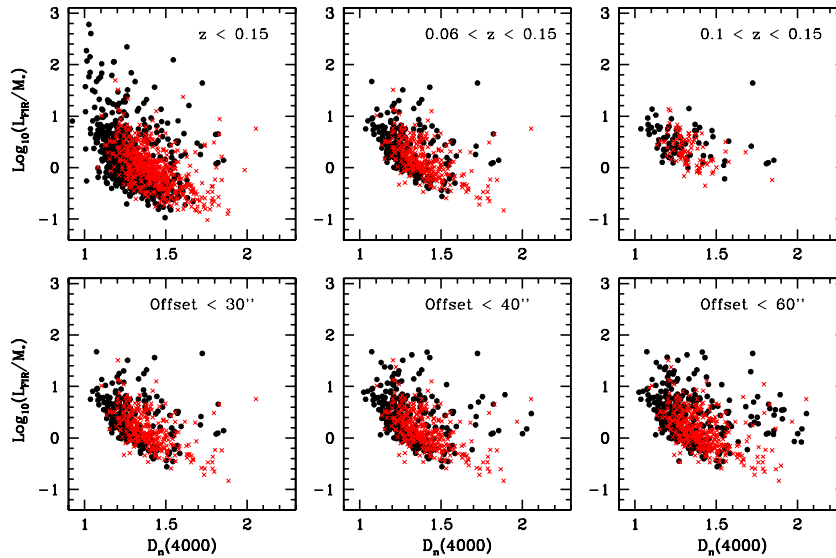


Figure 5. Top: The relation between normalized IR luminosity and 4000 Å break strength for different cuts in redshift. The positional offset is fixed to be $R < 30$ arcseconds. Bottom: The relation is shown for different cuts in positional offset while holding the redshift cut fixed at $0.06 < z < 0.15$. Red crosses indicate AGN of Type 2 and black dots normal star-forming galaxies.

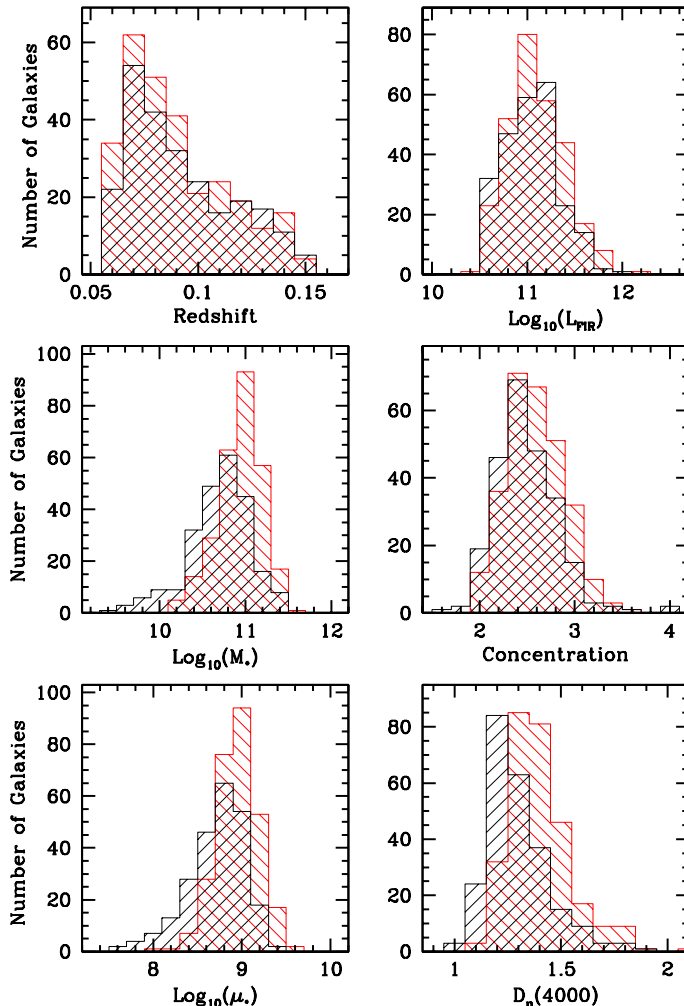


Figure 6. The distribution of IRAS-selected galaxies as a function of redshift, $\log L_{\text{FIR}}$, stellar mass M_* , concentration index C , stellar surface mass density μ_* and 4000 Å break strength $D_n(4000)$. The histograms of normal star-forming galaxies and AGN of Type 2 are shaded in black and in red, respectively.

in Kauffmann et al. (2003b), more massive galaxies have higher concentrations and surface densities and their stellar populations are also older. It is therefore not surprising that Figure 6 shows that the AGN are biased to higher values of C , μ_* and $D_n(4000)$ when compared to the star-forming galaxies.

In Figure 7, we plot the “normalized” IR-luminosity L_{FIR}/M_* as a function of stellar mass, concentration, stellar surface mass density and 4000 Å break strength. Once again solid black points indicate normal galaxies and red crosses AGN. It should be noted that the strong correlation between L_{FIR}/M_* and stellar mass and surface density is a selection effect caused by our redshift cut and by the IRAS flux detection limit. However, it is possible to conclude from this plot that the *largest* normalized IR-luminosities are obtained for galaxies with the lowest masses, concentrations and surface densities. There are few AGN in this region of parameter space. At a *fixed* value of M_* , C or μ_* , however, the differences between AGN and non-AGN are much more subtle. There does not appear to be a significant difference between the normalized IR-luminosities of AGN and non-

AGN at fixed stellar mass or concentration, but AGN do appear to be offset to slightly higher values of L_{FIR}/M_* at a fixed value of $D_n(4000)$.

We now divide our samples of AGN and normal star-forming galaxies (non-AGN) into bins of stellar mass with a width of $\Delta\text{Log}_{10}(M_*) = 0.2$. We only consider bins that contain at least 10 AGN and 10 normal star-forming galaxies. We compute the mean $\text{Log}_{10}(L_{\text{FIR}}/M_*)$ of the AGN and the normal star-forming galaxies in each bin and we define the “AGN excess” $\Delta\text{Log}_{10}(L_{\text{FIR}}/M_*)$ as

$$\langle\text{Log}_{10}(L_{\text{FIR}}/M_*)\rangle_{\text{AGN}} - \langle\text{Log}_{10}(L_{\text{FIR}}/M_*)\rangle_{\text{non-AGN}}$$

To analyze whether our results depend on wavelength, we have also calculated $\Delta\text{Log}_{10}(L_{100}/M_*)$ and $\Delta\text{Log}_{10}(L_{60}/M_*)$, which use only the 100 or 60 μm fluxes rather than the combination of the two quantities. Our results are shown in Figure 8. The error bars have been computed using standard bootstrap resampling techniques. As can be seen, at a fixed stellar mass there is very little difference in normalized IR-luminosity between AGN and normal star-forming galaxies at any wavelength.

In the next step of the analysis, we divide our sample

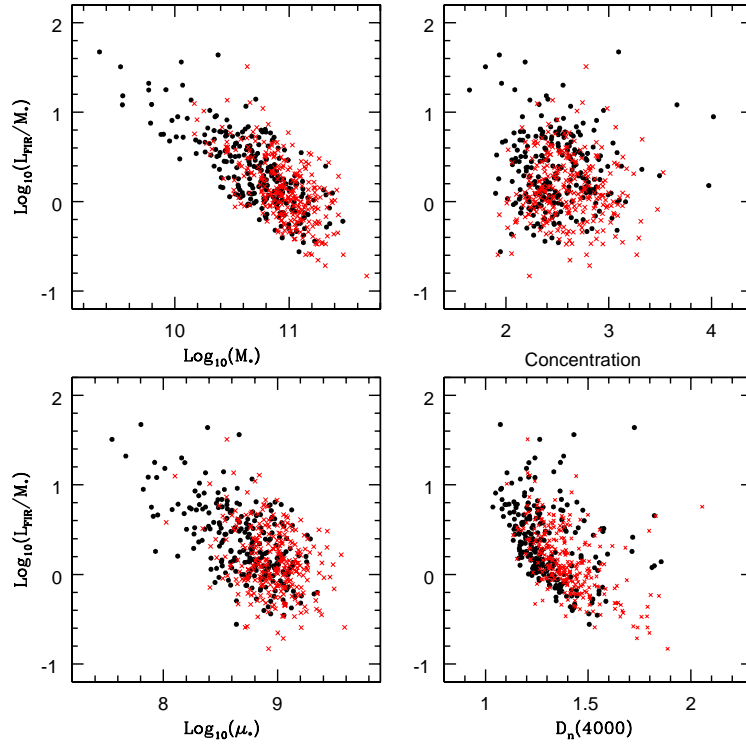


Figure 7. The normalized IR luminosity L_{FIR}/M_* is plotted as a function of stellar mass, concentration, stellar surface mass density and 4000 Å break strength for both normal star-forming galaxies (black points) and for AGN of Type 2 (red crosses).

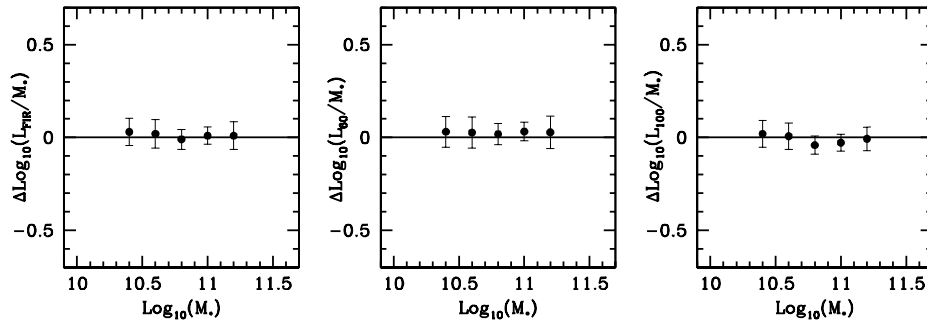


Figure 8. The difference between the average normalized IR luminosity of AGN of Type 2 and the average normalized IR luminosity of normal star-forming galaxies is calculated in bins of stellar mass M_* . Results are shown for L_{FIR} and well as for L_{60} and L_{100} .

into bi-dimensional bins in stellar mass *and* $D_n(4000)$. Once again, we only include bins with more than 10 AGN and normal star-forming galaxies in our analysis. The adopted bin sizes are 0.5 dex in $\log M_*$ and 0.1 in $D_n(4000)$. The left hand panels of Figure 9 show histograms of the distribution of $\Delta\text{Log}_{10}(L_{\text{FIR}}/M_*)$, $\Delta\text{Log}_{10}(L_{60}/M_*)$, and $\Delta\text{Log}_{10}(L_{100}/M_*)$ for the bins with sufficient galaxies and AGN to perform the comparison. In the right hand panels, the same quantities are plotted as a function of the value of $D_n(4000)$ at the center of each bin. We conclude that if galaxies and AGN are matched in both stellar mass and 4000 Å break strength, AGN tend to be brighter than star-forming galaxies by an amount which is larger at 60 μm than at 100 μm . However, this infrared excess is significant at a 2σ level at 60 μm and only at 1σ level at 100 μm and in L_{FIR} . The reason the excess is not seen in Figure 8 is be-

cause AGN are found in galaxies with larger 4000 Å break strengths than star-forming galaxies of the same mass.

4 MATCHED PAIR ANALYSIS

The differences between Figures 8 and 9 teach us that in order to compare the far-IR properties of AGN and normal star-forming galaxies in an unbiased way, it is important to match the properties of the host galaxies of these two kinds of systems as closely as possible. The relatively small number of galaxies in our sample means that it is not feasible to bin in more than two dimensions. Instead, we choose to create a sample of galaxy-AGN *pairs* that are closely matched in stellar mass M_* , $D_n(4000)$, concentration index C , stellar surface mass density μ_* (hence physical size) and redshift z .

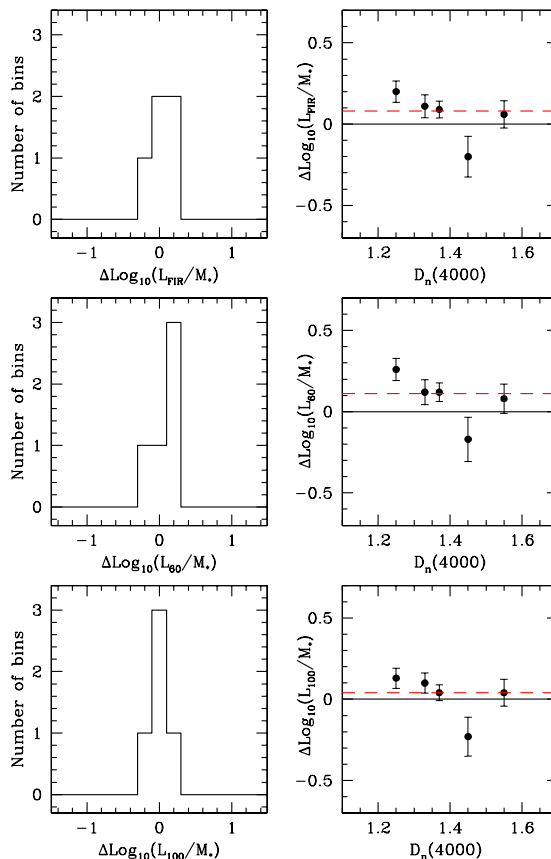


Figure 9. The difference between the average normalized IR luminosity of AGN of Type 2 and the average normalized IR luminosity of normal star-forming galaxies is calculated in bins of stellar mass and $D_n(4000)$. The left panels show histograms of the offset values and in the right panels, the offsets are plotted as a function of $D_n(4000)$ at the center of the bin. Results are shown for L_{FIR} , L_{60} and L_{100} . The dashed red line indicates the average value of offset. The errorbars correspond to 1σ .

In order to maximize the number of pairs, we first analyze the catalogue with reliable flux measurements at $60\ \mu\text{m}$. We accept pairs if $\Delta \log M_* < 0.25$, $\Delta D_n(4000) < 0.04$, $\Delta C < 0.1$, $\Delta \log \mu_* < 0.25$ and $\Delta z < 0.03$. This leaves us with a sample of 254 unique galaxy-AGN pairs.

In Figure 10, we plot $\Delta \log L_{60}/M_*$ (the difference between the normalized $60\ \mu\text{m}$ luminosity of the AGN and the matched galaxy) for each pair as a function of a number of parameters describing the AGN. The red points on the plot show the average value of $\Delta \log L_{60}/M_*$ calculated in bins of each parameter (the red point is positioned at the center of the bin). The close pair analysis indicates that there is a 0.2 dex excess in $\Delta \log L_{60}/M_*$ for the AGN relative to the normal star-forming galaxies. The excess does not depend on redshift (showing that is not caused by aperture effects) or on structural properties such as galaxy concentration or stellar surface mass density. It does appear to be larger for lower mass AGN with smaller $4000\ \text{\AA}$ breaks and for more powerful AGN with larger extinction-corrected [OIII] luminosities.

In order to assess the error in the measured far-IR excess of AGN, we generated 5 different galaxy/AGN pair samples by starting the search for pairs from different points in the catalogue. In addition, we created 300 bootstrap resamplings of each of the 5 pair samples in order to assess whether our results were sensitive to the presence of a few outliers in

Table 1. The results of the bootstrap technique applied to the $60\ \mu\text{m}$ catalogue.

Sample	Excess at $60\ \mu\text{m}$	1σ error
1	0.208	0.0327
2	0.174	0.0213
3	0.205	0.0331
4	0.180	0.0194
5	0.204	0.0324

the distribution. The derived $60\ \mu\text{m}$ excess for each of the 5 samples and the associated error estimated from the bootstrap resamplings are listed in Table 1. As can be seen, the variance among the 5 samples is consistent with the errors calculated using the bootstrap technique and is around 0.03 dex. We thus conclude that our measured $60\ \mu\text{m}$ excess of 0.2 dex is statistically significant. In the same way, we derived an error of 0.035 dex on the excess measured at $100\ \mu\text{m}$ and in L_{FIR} . This implies that the excesses found at 60 and $100\ \mu\text{m}$ differ at about the 2σ level.

Figure 11 shows histograms of the distribution of $\Delta \log L_{60}/M_*$, $\Delta \log L_{100}/M_*$ and $\Delta \log L_{FIR}/M_*$. Note that the results for L_{100} and L_{FIR} are based on a sample of 111 pairs from the catalogue with reliable flux measure-

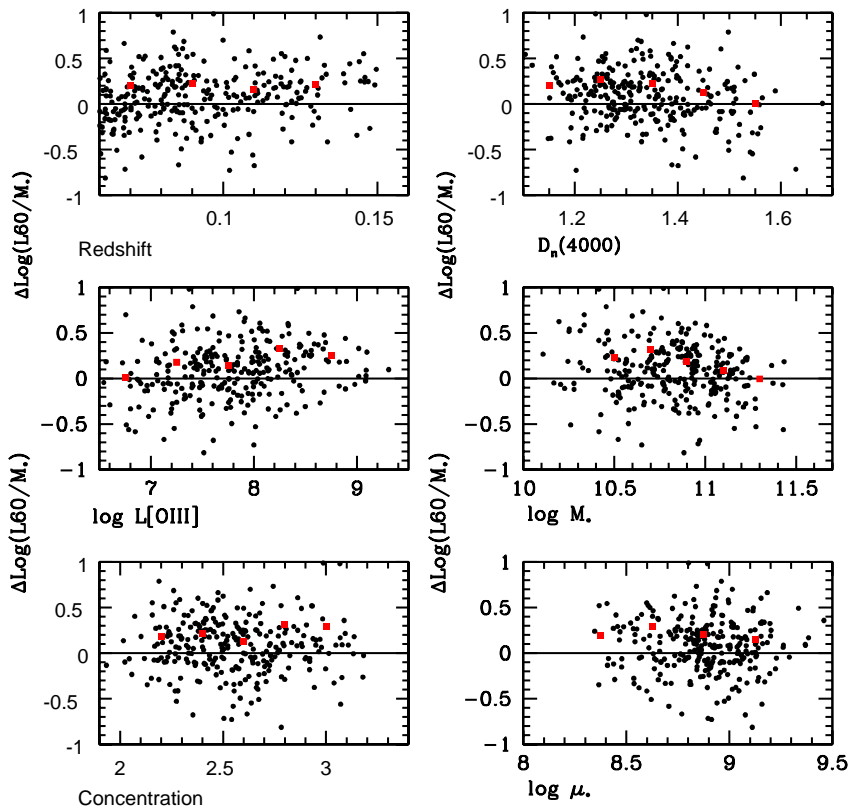


Figure 10. The difference between the normalized 60 μm IR luminosity of an AGN of Type 2 and a matching normal star-forming galaxy is plotted for a sample of 254 galaxy-AGN pairs. The difference is shown as a function of the redshift, 4000 \AA break strength, extinction-corrected [OIII] luminosity, stellar mass, concentration and stellar surface density of the AGN in each pair. Red symbols indicate the average value of $\Delta \log L_{60}/M_*$ evaluated in bins of each of these 6 parameters.

ments in both the 60 and 100 μm bands. Fig. 11 demonstrates the excess IR emission in AGN is larger at 60 μm than at 100 μm .

5 INTERPRETATION AND DISCUSSION

We have demonstrated that when IRAS-selected AGN and normal star-forming galaxies are carefully matched in terms of parameters such as stellar mass, size, concentration, redshift and 4000 \AA break, the AGN exhibit “excess” far-IR emission of about 0.18 dex in $\log L_{\text{FIR}}/M_*$.

What causes this excess emission in AGN? One possibility is that the excess originates from the active nucleus itself. The question one might then ask is whether this is energetically feasible. In Type 2 AGN, the central engine is obscured and the AGN luminosity can only be estimated indirectly. Heckman et al. (2004) have discussed how the [OIII] luminosity can be used as a tracer of AGN activity. They used the bolometric correction to the [OIII] luminosity derived for Type 1 AGN to estimate the average mass accretion rate onto black holes in the local Universe. The implied bolometric correction was $L_{\text{Bol}}/L_{\text{O3}} \sim 3500$, where L_{O3} was the [OIII] luminosity in solar units, uncorrected for extinction due to dust. The quoted uncertainty on this conversion was ~ 0.4 dex.

In the left panel of Figure 12, we plot L_{FIR} as a function of the raw, uncorrected [OIII] luminosity for the AGN

in our sample with reliable flux densities at 60 and 100 μm . We have found that these AGN have on average a 0.18 dex excess in $\log L_{\text{FIR}}/M_*$. This would imply that one third of the total FIR luminosity is from the AGN. In the left panel of Figure 12, we see that the median ratio of FIR to [OIII] luminosity is 5 dex. In the assumption that the quoted 0.18 dex excess in $\log L_{\text{FIR}}/M_*$ is entirely due to the AGN, a FIR-[OIII] luminosity ratio of 5 dex would imply a typical ratio of FIR (AGN) to [OIII] of several 10^4 . This is about an order-of-magnitude greater than the entire bolometric luminosity of the AGN if we assume the bolometric correction of Heckman et al. At first glance, this would appear to rule out the hypothesis that the observed excess could be produced by the active nucleus. We caution, however, that our IRAS-selected AGN are not typical of the general population of AGN in the SDSS spectroscopic sample. In particular, they have considerably higher $\text{H}\alpha/\text{H}\beta$ ratios, which implies that the amount of extinction for the [OIII] line is larger. In the right hand panel of Figure 12 we plot L_{FIR} as a function of the *extinction-corrected* [OIII] luminosity. The average extinction correction to [OIII] for the AGN in our sample is a factor of ~ 100 . This is five times larger than the correction derived for the general population of SDSS AGN with raw [OIII] luminosities in the same range as those in our SDSS/IRAS sample. It is not unreasonable to suppose that strong systematic effects may arise when applying a calibration derived for “typical” Type 1 AGN to a sample of very dusty Type 2 AGN. Figure 12 shows that if the extinction

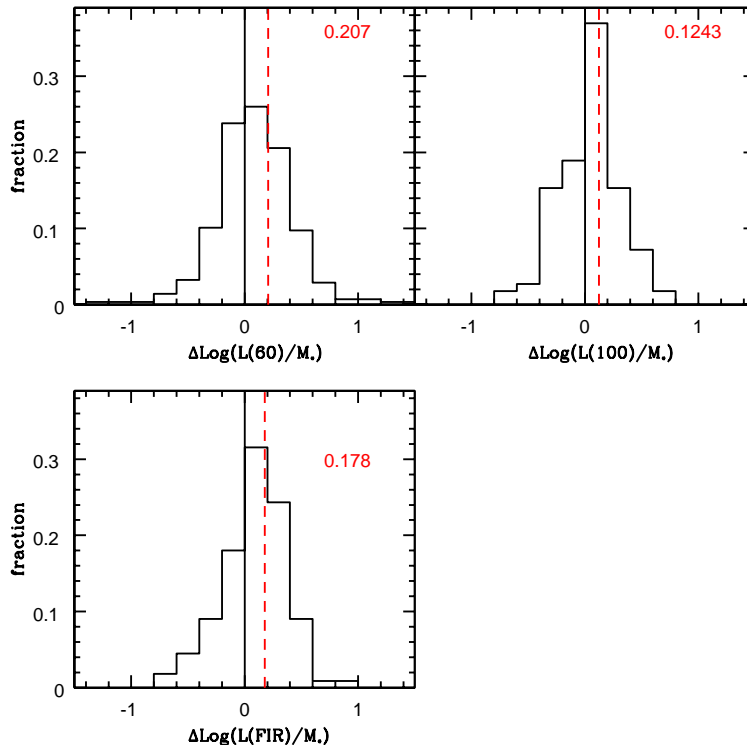


Figure 11. Histograms of the difference between the normalized IR luminosity of an AGN of Type 2 and a matching normal star-forming galaxy are plotted for samples of galaxy-AGN pairs. Results are shown for the 60 μm , 100 μm and FIR luminosities. The average value of $\Delta \log L/M_*$ is indicated by the red dashed line and its value is given in the top right corner of each panel.

correction is applied, the median ratio of FIR to [OIII] luminosity is ~ 3 dex. The FIR excess attributed to the AGN would now be only several hundred times the extinction-corrected [OIII] luminosity. This is still rather large to account for the measured infrared excess of AGN.

An alternative explanation is that the excess infrared emission is caused by an extra component of star formation, which is not reflected in the measured 4000 \AA break strengths. Kauffmann et al. (2003) showed that the distribution of AGN with strong [OIII] emission in the plane of $H\delta$ absorption line strength versus 4000 \AA break strength was systematically different than that of ordinary star-forming galaxies of the same stellar mass. The AGN were offset to higher values of $H\delta_A$ at a given value of $D_n(4000)$, indicating that they were more likely to have experienced a recent burst of star formation. In the left panel of Figure 13, we compare the $H\delta$ equivalent widths of IRAS-selected AGN and normal star-forming galaxies and find that there is no significant offset in mean equivalent width between the two populations. Both populations are characterized by strong $H\delta$ absorption lines and irregular morphologies (Pasquali et al., in preparation) and we conclude that IRAS selection favours galaxies with bursty star formation histories irrespective of whether or not they are classified as an AGN. If there is an excess component of star formation in the AGN in our sample, it clearly cannot be detected using standard indicators in the optical part of the spectrum. In the left panel of Fig. 13, we compare the Balmer decrements of the AGN and the normal star-forming galaxies. The AGN exhibit a small offset towards larger values of $H\alpha/H\beta$. This may indicate that AGN contain slightly more dust, but an

offset in this direction is also expected because of the different ionization conditions in these systems. The offset in Balmer decrement between AGN and normal star-forming galaxies is not sufficient to explain the offset in FIR luminosity; we have verified this by creating AGN/galaxy samples that are closely matched in redshift (< 0.03), stellar mass (< 0.25 dex), $D4000$ (< 0.07) and $H\alpha/H\beta$ (< 0.005 dex) and we find that the mean offset in L_{FIR}/M_* changes very little.

At infrared wavelengths, the only diagnostics available to us are the IRAS 60 and 100 μm fluxes. It is possible to study whether AGN exhibit a greater degree of scatter in their far-IR properties relative to normal star-forming galaxies. We have created samples of AGN/AGN and galaxy/galaxy pairs using the exact same matching criterion used for the galaxy/AGN pairs. We then compare the scatter in 60 μm luminosity differences for the two pair samples. Figure 14 presents the results of this analysis and shows clearly that the AGN exhibit greater spread in their IR luminosities than the star-forming galaxies in our sample. This is consistent with the idea that the star formation in AGN is more episodic but it does not prove the hypothesis that an excess population of young stars is present in the AGN. One could imagine that dust heating by the central source might also be subject to temporal fluctuations. What is required in order to understand our results in more detail is high resolution imaging of these galaxies at infrared or radio wavelengths. This would enable us to compare the distributions of the dust emission and star-forming sites in the two classes of galaxies. With the combination of spatial information and good statistics, it should be possible to dis-

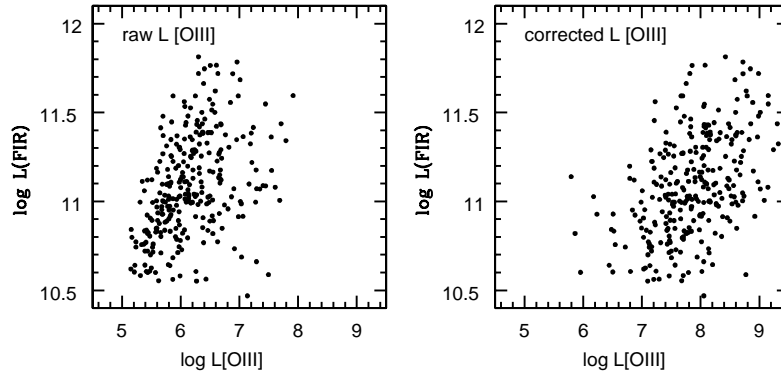


Figure 12. Left: The FIR luminosities of IRAS-selected AGN of Type 2 are plotted as a function of their raw (uncorrected) [OIII] luminosities. Right: The FIR luminosities are plotted as a function of extinction corrected L[OIII].

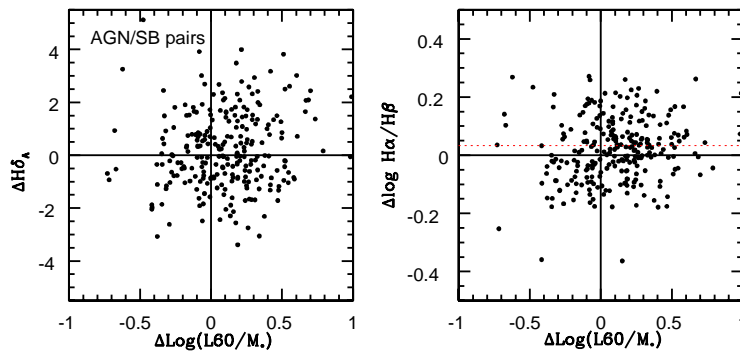


Figure 13. Left: The difference between $H\delta_A$ index strength is plotted as function of $\Delta L_{60}/M_*$ for matched galaxy/AGN pairs. Right: The difference in the logarithm of the Balmer decrement is plotted as function of $\Delta L_{60}/M_*$ (the red dotted line indicates the average value of the difference).

entangle the physical mechanisms responsible for the excess far-infrared emission observed in nearby Seyfert 2 galaxies.

ACKNOWLEDGMENTS

We would like to thank S. Charlot and C. Tremonti for helpful discussions, and an anonymous referee for useful comments that improved the paper.

Funding for the creation and distribution of the SDSS Archive has been provided by the Alfred P. Sloan Foundation, the Participating Institutions, the National Aeronautics and Space Administration, the National Science Foundation, the U.S. Department of Energy, the Japanese Monbukagakusho, and the Max Planck Society. The SDSS Web site is <http://www.sdss.org/>.

The SDSS is managed by the Astrophysical Research Consortium (ARC) for the Participating Institutions. The Participating Institutions are The University of Chicago, Fermilab, the Institute for Advanced Study, the Japan Participation Group, The Johns Hopkins University, Los Alamos National Laboratory, the Max-Planck-Institute for Astron-

omy (MPIA), the Max-Planck-Institute for Astrophysics (MPA), New Mexico State University, University of Pittsburgh, Princeton University, the United States Naval Observatory, and the University of Washington.

REFERENCES

- Armus, L., Heckman, T.M., Miley, G.K., 1990, ApJS, 74, 833
- Barger, A.J., Cowie, L.L., Steffen, A.T., Hornschemeier, A.E., Brandt, W.N., Garmire, G.P., 2001, ApJ, 560, L23
- Blain, A.W., Smail, I., Ivison, R., Kneib, J.-P., 1999, MNRAS, 302, 632
- Brinchmann, J., Charlot, S., White, S.D.M., Tremonti, C., Kauffmann, G., Heckman, T.M., Brinchmann, J., 2004, MNRAS, 351, 1151
- Brinchmann, J., Charlot, S., Heckman, T.M., Kauffmann, G., Tremonti, C., White, S.D.M., 2004, astro-ph/0406220
- Cid Fernandes, R., Heckman, T., Schmitt, H., Delgado, R.M. Gonzalez, Storchi-Bergmann, T., 2001, ApJ, 558, 81
- Condon, J.J., Huang, Z.P., Yin, Q.F., Thuan, T.X., 1991, ApJ, 378, 65
- De Grijp, M.H.K., Miley, G.K., Lub, J., De Jong, T., 1985, Nature, 314, 240

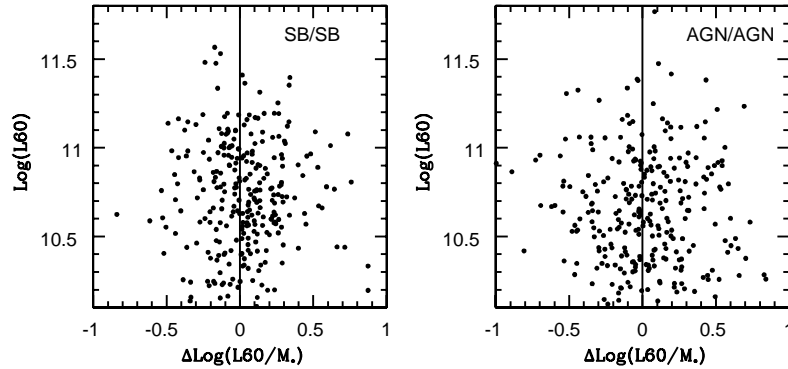


Figure 14. The difference in normalized 60 μm luminosity is plotted as a function of $L(60)$ for a sample of matched pairs of normal star-forming galaxies (left) and AGN of Type 2 (right).

- De Grijp, M.H.K., Keel, W.C., Miley, G.K., Goudfrooij, P., Lub, J., *A&AS*, 96,389
- Genzel, R., Lutz, D., Sturm, E., Egami, E., Kunze, D., Moorwood, A.F.M., Rigopoulou, D., Spoon, H.W.W. et al., 1998, *ApJ*, 498, 579
- Granato, G.L., Danese, L., 1994, *MNRAS*, 268,235
- Heckman, T.M., Kauffmann, G., Brinchmann, J., Charlot, S., Tremonti, C., White, S.D.M., 2004, *ApJ*, 613, 109
- Helou, G., Khan, I.R., Malek, L., Boehmer, L., 1988, *ApJS*, 68, 151
- Kauffmann, G., Heckman, T.M., White, S.D.M., Charlot, S., Tremonti, C., Brinchmann, J., Bruzual, G., Peng, E.W. et al., 2003a, *MNRAS*, 341, 33
- Kauffmann, G., Heckman, T.M., White, S.D.M., Charlot, S., Tremonti, C., Peng, E.W., Seibert, M., Brinkmann, J. et al., 2003b, *MNRAS*, 341, 54
- Kauffmann, G., Heckman, T.M., Tremonti, C., Brinchmann, J., Charlot, S., White, S.D.M., Ridgway, S.E., brinkmann, J. et al., 2003c, *MNRAS*, 346, 1055
- Kewley, L., Jansen, R.A., Geller, M.J., 2005, *PASP*, 117, 227
- Pier, E.A., Krolak, J.H., 1992, *ApJ*, 401,99
- Rieke, G.H., Cutri, R.M., Black, J.H., Kailey, W.F., McAlary, C.W., Lebofsky, M.J., Elston, R., 1985, *ApJ*, 290, 116
- Rowan-Robinson, M., Crawford, J., 1989, *MNRAS*, 238, 523
- Rowan-Robinson, M., 2001, *ApJ*, 549, 745
- Sanders, D.B., Soifer, B.T., Elias, J.H., Neugebauer, G., Matthews, K., 1988, *ApJ*, 328, L35
- Sanders, D.B., Mirabel, I.F., 1996, *ARA&A*, 34, 749
- Severgnini, P., Maiolino, R., Salvati, M., Axon, D., Cimatti, A., Fiore, F., Gilli, R., La Franca, F. et al., 2000, *A&A*, 364, 348
- Silva, L., Maiolino, R., Granato, G.L., 2004, *MNRAS*, 335, 973
- Strateva, I., Ivezić, Ž., Knapp, G.R., Narayanan, V., Strauss, M., Gunn, J., Lupton, R., Schlegel, D. et al., 2001, *AJ*, 122, 1861
- Stoughton, C., Lupton, R., Bernardi, M., Blanton, M., Burles, S., Castander, F., Connolly, A., Eisenstein, D. et al. 2002, *AJ*, 123, 485
- Tremonti, C.A., Heckman, T.M., Kauffmann, G., Brinchmann, J., Charlot, S., White, S.D.M., Seibert, M., Peng, E.W. et al. 2004, *ApJ*, 613, 898
- York, D.G. et al. 2000, *AJ*, 120, 1579